UV and Temperature-Sensing Based on NaGdF$_4$:Yb^{3+}:Er^{3+}@SiO$_2$–Eu(tta)$_3$

Karina Nigoghossian,[†,‡,§] Younès Messaddeq,[†,‡] Denis Boudreau,[‡,§] and Sidney J. L. Ribeiro*,[†]

[†]Laboratory of Photonic Materials, Institute of Chemistry, São Paulo State University, UNESP, CP 355, Araraquara, São Paulo 14801-970 Brazil

[‡]Centre d'optique, photonique et laser and [§]Department of Chemistry, Université Laval, Québec, Québec G1V 0A6, Canada

ABSTRACT: A multifunctional nanosystem was synthesized to be used as a dual sensor of UV light and temperature. NaGdF$_4$:Yb^{3+}:Er^{3+} upconverting nanoparticles (UCNPs) were synthesized and coated with a silica shell to which a europium(III) complex was incorporated. The synthesis of NaGdF$_4$ UCNPs was performed via thermal decomposition of lanthanide ion fluoride precursors in the presence of oleic acid. To achieve sufficient water dispersibility, the surface of the hydrophobic oleate-capped UCNPs in the hexagonal phase was modified by a silica coating through a modified Stöber process through a reverse microemulsion method. An Eu(tta)$_3$ (tta: thenoyltrifluoroacetonate) complex was prepared in situ at the silica shell. A dual-mode nanothermometer was obtained from a near infrared to visible upconversion fluorescence signal of Er^{3+} ions together with UV-excited downshifting emission from the Eu^{3+} complex. Measurements were recorded near the physiological temperature range (293–323 K), revealing excellent linearity ($R^2 > 0.99$) and relatively high thermal sensitivities ($\geq 1.5\%\cdot K^{-1}$). The Eu(tta)$_3$ complex present in the silica shell was tested as the UV sensor because of the Eu^{3+} luminescence dependence on UV-light exposure time.
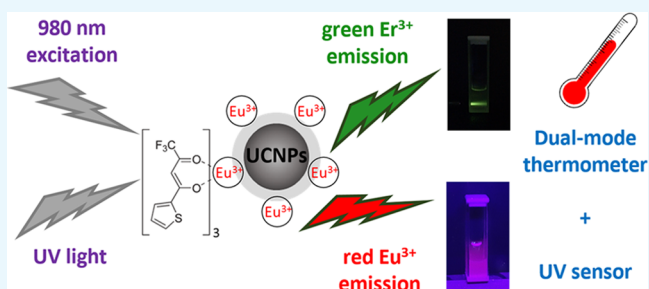
1. INTRODUCTION

The rapid advance in nanotechnology has enabled the development of materials that integrate multiple functions, each one related to their components that act synergistically. A large number of composite nanomaterials have been created, which exhibit excellent chemical, physical, and biological properties with strong potential in biomedicine,[1] catalysis,[2] sensors,[3] energy conversion,[4] and so forth. Incorporation of luminescent species in such materials gives rise to additional applications in photonics, medicine, sensing, and imaging as well. In fact, lanthanide-based materials possess special luminescence properties such as narrow photoluminescence peaks, tunable photostability, relatively high emission quantum yields, and emission lines spanning the electromagnetic spectrum from the ultraviolet to the infrared region, allowing high-technology applications.[5−8]

One interesting application of the luminescent properties of lanthanide ions consists of thermometry on the nanoscale because of a strongly temperature-dependent effect.[9−11] Temperature is a fundamental variable that governs diverse intracellular chemical and physical interactions in the life cycle of biological cells.[12] Measuring the temperature of cancer cells at the cellular level, for example, allows the optimization of therapeutic processes (e.g., hyperthermal tumor treatment).[13,14] Another current interest in nanothermometry is monitoring temperature in micro- or nanoelectronics "hot spots".[15,16] Fundamental properties such as the instantaneous ballistic velocity of suspended Brownian nanocrystals have been

measured with nanothermometers as well.[17] Temperature variations may induce different effects on the luminescence of lanthanides, including (i) redistribution of the electronic state population due to Boltzmann statistics, (ii) quenching mechanisms that result in decreasing emission intensity, and (iii) nonradiative transition because of electron–phonon interactions.[18]

Several dopant ions have been used in lanthanide-based thermometers. Er^{3+}-containing materials present a strong temperature dependence on the relative intensity of its two green luminescence bands. This effect is associated with the thermal equilibrium in the population of excited states $^2H_{11/2}$ and $^4S_{3/2}$.[19] An interesting point relates to the fact that the green emission can be observed with excitation either in the UV or in the infrared region. In the latter case, the so-called upconversion emission is treated. It is a well-known feature observed for many different lanthanide ions, being used in several different fields.[20−22] Concerning the UV-excited down-shifting emission of Eu^{3+} complexes with organic ligands, a temperature probe with a highly temperature-dependent emission is related to the thermal deactivation of the $^5D_0$ excited state.[23−26] Eu^{3+} complexes may also present an additional issue that is related to their reduced photostability under UV irradiation. Because UV light detection is of great

interest in environmental and biological fields, among others, the low photostability may be well explored for UV dose sensing.[27−34] Therefore, dual-modal temperature sensors may be obtained from two active centers with different temperature-sensitive luminescence features. Such thermometers may combine two lanthanide ions.[35−37] The second probe may be an organic dye,[38] a quantum dot,[39] or a transition metal ion.[40−46]

Lanthanide-based upconversion nanoparticles (UCNPs) are a promising solution for biological systems as they can be excited in the near infrared (NIR) region within the biological transparency window and emit NIR photons or higher energy (visible) photons. High penetration depths and low auto-fluorescence are some of the unique advantages related to the use of low-energy NIR excitation photons compared with conventional luminescent nanomaterials, such as organic dyes and quantum dots, which require an excitation source in the UV−visible region.[47]

This work proposes a multifunctional nanoplatform that combines two independent luminescent probes. NaGd-F$_4$:Yb^{3+}:Er^{3+}@SiO$_2$−Eu(tta)$_3$ nanoparticles were prepared as a temperature sensor in the vicinity of the biological range (293−323 K) and a UV-light detector.

2. METHODS

2.1. Materials.
Lanthanide oxides (gadolinium oxide, ytterbium oxide, and erbium oxide), europium(III) chloride hexahydrate, trifluoroacetic acid, sodium trifluoroacetate, oleic acid, 1-octadecene, IGEPAL CO-520, ammonium hydroxide (28−30%), tetraethyl orthosilicate (TEOS), and 2-thenoyltrifluoroacetone (tta) were all purchased from Sigma (Sigma-Aldrich Co., St. Louis, MO, USA).

2.2. Synthesis of Yb^{3+}/Er^{3+} Co-Doped NaGdF$_4$ UCNPs.
The synthesis of colloidal NaGdF$_4$ upconverting nanoparticles doped with the ions Yb^{3+}/Er^{3+} was performed via thermal decomposition of fluoride precursors of lanthanide ions. The method described previously by Hemmer et al.[48] is a two-pot synthesis. In the first step of the synthesis, the lanthanide trifluoroacetate precursor was prepared. A 10 mL mixture of trifluoroacetic acid and water (1:1) was added to a 50 mL three-neck round bottom flask containing gadolinium oxide (353.4 mg, 0.975 mmol), ytterbium oxide (98.5 mg, 0.250 mmol), and erbium oxide (9.6 mg, 0.025 mmol) to obtain a molar ratio of Gd:Yb:Er = 78:20:2. The solution was refluxed at 353 K for 12 h until a clear solution was obtained. The temperature was then lowered to 333 K, and the flask was opened to let water and trifluoroacetic acid evaporate to dryness for 5 h. In the second step, 340 mg of sodium trifluoroacetate was added to the flask in which the precursor lanthanide trifluoroacetate was previously prepared, followed by the addition of 7.5 mL each of oleic acid and 1-octadecene. In a second flask (a three-neck round bottom flask of 100 mL), 12.5 mL each of oleic acid and 1-octadecene were added. The flasks were connected to a Schlenk line to remove moisture and oxygen for 30 min at 125 °C under vacuum and magnetic stirring. Subsequently, the flask containing oleic acid and 1-octadecene was heated to 583 K under argon flow at a heating rate of 10 K/min. A few minutes after reaching this temperature, the precursor solution at 398 K was collected with a glass syringe and injected dropwise to the reaction vessel. A pump system was used at an injection rate of 1.5 mL min^{-1}. The solution was maintained at 583 K for a further 60 min under stirring and argon flow. After this period, the heating

source was removed. When the solution reached room temperature, the obtained nanoparticles were precipitated by the addition of ethanol and centrifuged at 5350 RCF for 10 min. The nanoparticles were washed twice by dispersing in hexane, followed by precipitation with ethanol (1:5 v/v), and then recovered using centrifugation. The resultant oleate-capped NaGdF$_4$:Yb^{3+}:Er^{3+} nanoparticles were finally redispersed in hexane for further characterizations.

2.3. Silica Coating of NaGdF$_4$:Yb^{3+}:Er^{3+} UCNPs.
The obtained UCNPs were coated with a silica shell using a reverse microemulsion method.[49] First, 32 mg of UCNPs were dispersed in 10 mL of cyclohexane, and then 0.4 g of the surfactant IGEPAL CO-520 was added. After 10 min of stirring, 1.6 g of IGEPAL CO-520 and 80 μL of ammonium hydroxide were added to form a water-in-oil microemulsion. The emulsion was sonicated for 30 min. TEOS (40 μL) was then added and the solution was stirred at 300 rpm for 48 h. The nanoparticles were precipitated by adding acetone and washed twice with ethanol/water (1:1). Centrifugation was performed to recover the particles at 1590 RCF for 20 min. The UCNP core−silica shell (UCNPs@SiO$_2$) was finally stored in water.

2.4. Preparation of NaGdF$_4$:Yb^{3+}:Er^{3+}@SiO$_2$−Eu(tta)$_3$.
First, europium was incorporated in the silica shell by adding europium(III) chloride hexahydrate solution in ethanol (1.5 mL, 20 mM) to UCNPs@SiO$_2$ (10 mg). The mixture was placed in an ultrasonic bath for 1 h and then 24 h under stirring in a vortex mixer. The nanoparticles were separated using centrifugation (1590 RCF/20 min). Afterward, the ligand tta was added in a 3:1 molar ratio tta/Eu. An ethanolic tta solution (1.5 mL, 60 mM) was added to the recovered particles and then dispersed using ultrasound followed by the addition of ammonia solution (75 μL). Stirring was continued for 24 h in a thermomixer (Eppendorf) at 800 rpm and 281 K. The particles were centrifuged (1590 RCF/20 min) and washed once with ethanol and once with hexane and finally suspended in ethanol (1.5 mL).

2.5. Characterization.
A Tecnai G2 Spirit BioTwin (120 kV) transmission electron microscope (TEM) was used to analyze the particle size and structural morphology. The crystal phase of the UCNPs was investigated by X-ray diffraction (XRD) using a Siemens D5000 Kristalloflex diffractometer using nickel-filtered Cu Kα radiation. The processing software was JADE version 2.1 coupled with the JCPDS (Joint Committee on Powder Diffraction Standards) database of ICDD (International Centre for Diffraction Data) 2001 version. UV-excited visible photoluminescence and NIR-excited upconversion emission spectra were measured using a FluoroLog-3 spectrofluorimeter (model 322) from HORIBA Jobin Yvon. A Xenon lamp and an external 980 nm continuous wave diode laser JDS Uniphase (model S26-7602-340) were used as excitation sources. The excitation power densities at the sample position were estimated by using a power meter (Newport 2935-C). To obtain the thermal calibration curves, the emission spectra were measured at different temperatures in a Peltier-based temperature-controlled cuvette holder coupled to the fluorometer. A period of 10 min was given to allow the temperature to stabilize. For upconversion emission spectra measured at different temperatures, the laser power at the sample position was 81 mW. The calibration measurements for the UV light sensor were recorded at room temperature with a power density of 1.35 mW/cm^2.

3. RESULTS AND DISCUSSION

UCNPs were obtained as oleate-capped $NaGdF_4$:Yb^{3+}:Er^{3+} via thermal decomposition of lanthanide trifluoroacetate. TEM images of $NaGdF_4$:Yb^{3+}:Er^{3+} (Figure 1a) show that mono-
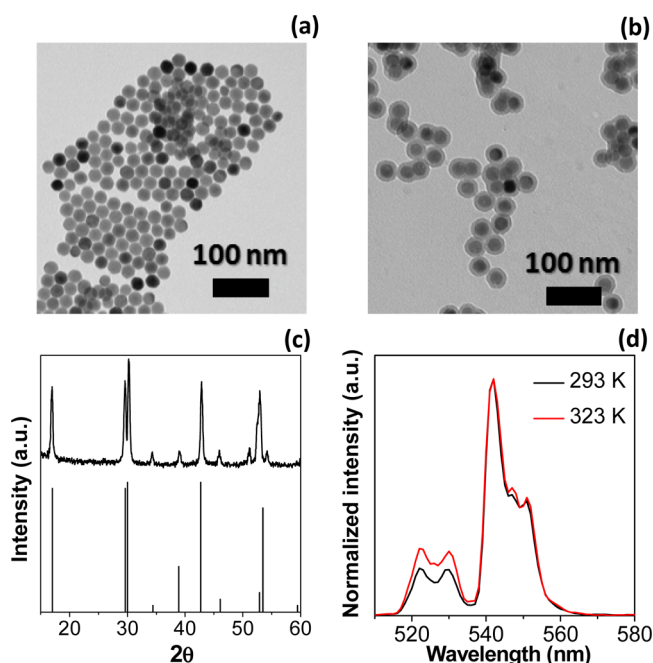

Figure 1. TEM images of (a) UCNPs and (b) UCNPs@SiO$_2$. (c) X-ray diffraction pattern and reference diffraction peaks corresponding to hexagonal $NaGdF_4$ (JCPDS file 27-0699). (d) Upconversion emission spectra (λ_{exc} 980 nm) at different temperatures (293 and 323 K) of UCNPs@SiO$_2$.

disperse nanocrystals (size 26.2 ± 1.7 nm) with hexagon-shaped morphology were obtained. The oleate-capped UCNPs are dispersible only in nonpolar solvents, such as hexane. The surface modification by a silica coating rendered the particles dispersible in water, which is important for biological applications. Additionally, silica is known to be highly stable, biocompatible, and optically transparent and to present abundant Si—OH active bonds available for surface functionalization; moreover, depending on the preparation method, high pore volumes may be obtained where different species may be stored.[50] TEM images of silica-coated UCNPs (Figure 1b) show a thin (approximately 7 nm thick) and uniform silica shell at the nanocrystal surface. An XRD pattern of oleate-capped $NaGdF_4$:Yb^{3+}:Er^{3+} and their corresponding phase reference graph of $NaGdF_4$ are presented in Figure 1c. The pattern is in accordance with the hexagonal phase (JCPDS file 27-0699), which is well known for its higher upconversion efficiency versus the cubic phase.[51] Figure 1d shows the upconversion emission spectrum (λ_{exc} 980 nm) of silica-coated UCNPs in water at two different temperatures (293 and 323 K). The bands observed in the spectral regions of 510–536 and 536–575 nm correspond to the Er^{3+} transitions $^2H_{11/2} \rightarrow {}^4I_{15/2}$ and $^4S_{3/2} \rightarrow {}^4I_{15/2}$, respectively. As the temperature increases, the relative emission intensity at approximately 523 nm was observed to increase with respect to the emission at 543 nm because of a thermally driven population increase in the higher energy level ($^2H_{11/2}$), to the detriment of the lower energy level ($^4S_{3/2}$). This effect is in accordance with the Boltzmann distribution as defined by eq 1

$$ \text{FIR} = \frac{I_{523}}{I_{543}} = C \exp\left(-\frac{\Delta E}{k_B T}\right) \tag{1} $$

where FIR is the fluorescence intensity ratio between the integrated intensities of the emission bands at 523 and 543 nm, represented by I_{523} and I_{543}, respectively; C is a constant that depends on the degeneracies and spontaneous emission rates of the emitting states and photon energies; and ΔE is the energy gap between the two excited states.

Figure 2 shows the photoluminescence excitation spectrum (PLE—Figure 2a) and photoluminescence emission spectrum
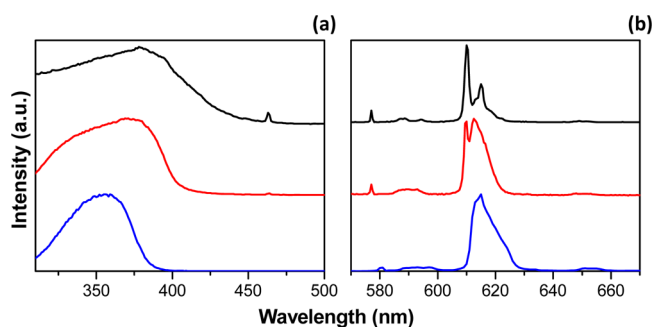

Figure 2. (a) Excitation (λ_{em} 615 nm) and (b) emission spectra for the complex $[Eu(tta)_3(H_2O)_2]$ (black), the compound $[Eu(tta)_3-host]$ (red), and UCNPs@SiO$_2$–Eu(tta)$_3$ (blue). Spectra of $[Eu(tta)_3(H_2O)_2]$ and $[Eu(tta)_3-host]$ were adapted from Molina et al.[52]

(PL—Figure 2b) obtained for $NaGdF_4$:Yb^{3+}:Er^{3+}@SiO$_2$–Eu(tta)$_3$ nanoparticles. Two spectra of the well-known complex $[Eu(tta)_3(H_2O)_2]$ and the compound $[Eu(tta)_3-U]$ (U stands for an ureasil organic–inorganic hybrid host) adapted from Molina et al.[52] are also shown for comparison purposes. The broad excitation band (with maximum at 352 nm) covering the region of the UV-A (400–315 nm) and UV-B (315–280 nm) in PLE spectra accounts for the antenna effect because of the presence of tta ligands. Similarities in spectra allow us to propose that the Eu(tta)$_3$ compound is formed at the silica nanoshell of the new nanoparticles. As already mentioned, the strong UV absorption cross section and efficient energy transfer make these Eu^{3+} complexes strong red light emitters. The well-known PL spectrum obtained for $[Eu(tta)_3(H_2O)_2]$ shows emission arising mainly from the Eu^{3+} $^5D_0$ to the ^7F_J manifold ($J = 0, 1, 2, 3, 4$), with the $^5D_0 \rightarrow {}^7F_2$ dominating the general intensity. When incorporated either in the organic–inorganic hybrid studied before or in the silica nanoshell of the present nanoparticles, broadening is observed because of the inhomogeneous distribution of sites in the two hosts.

The drawback that could hinder the practical application of these luminophores refers to low photostability of the β-diketonates under UV light.[27] However, one can take in advantage that property that can be useful for application as a sensor UV after exposure to sunlight.

Figure 3a shows nanoparticle emission spectra obtained in the temperature range of 293–323 K under UV irradiation. The inset shows a photograph of the cuvette under UV illumination. A decrease in the Eu^{3+} emission intensity is observed with the increase in temperature because of a competition between emission and nonradiative energy transfer from the Eu^{3+} ion to the ligand (Figure 3a). As mentioned in the Introduction, the utilization of the Eu^{3+}/tta species in temperature measurements based on intensity changes is well known.[23–26] Figure 3b shows

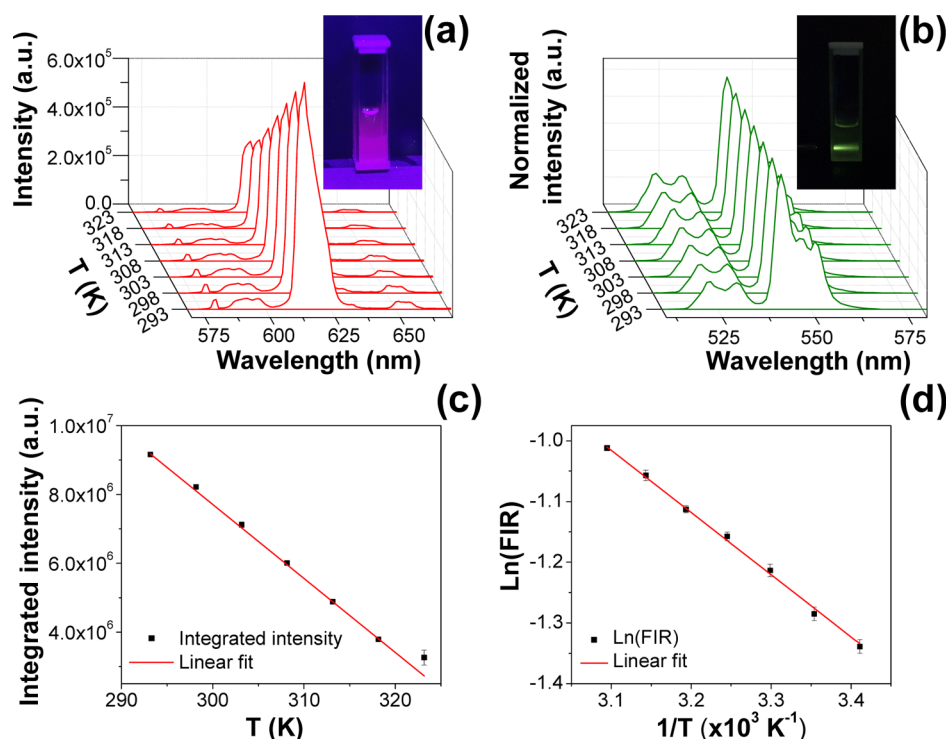**Figure 3.** Emission spectra of UCNPs@SiO$_2$−Eu(tta)$_3$ at different temperatures (293−323 K): under (a) UV and (b) NIR excitation. Insets: Corresponding luminescent photographs. Thermal calibration curves: (c) fluorescence intensity (integrated area) vs temperature (λ_{exc} 352 nm) and (d) ln(FIR) vs inverse temperature (λ_{exc} 980 nm).

the upconversion spectra in the same temperature range. The inset shows a photograph of the cuvette under 980 nm illumination. Here, again, the temperature-dependent variation of the emission lines can clearly be observed. Figure 3c,d show the linear correlations that can be obtained for both Eu^{3+} (λ_{exc} 352 nm, R^2 = 0.99965) and Er^{3+} (λ_{exc} 980 nm, R^2 = 0.99776) emission bands upon temperature variations. The integration ranges used to compute the integrated areas are 510−536 and 536−565 nm for Er^{3+} emissions and 603−643 nm for Eu^{3+} emission. For each temperature, the average of five measurements were calculated; the error bars in the plots represent standard deviation. A dual-mode temperature sensor is therefore proposed here. The energy gap between the ^{2}H$_{11/2}$ and ^{4}S$_{3/2}$ states of Er^{3+} was estimated from the slope of Boltzmann plot (Figure 3d), which gives the parameter $\Delta E/k_B$ (eq 1). The value calculated from the slope (724 cm^{-1}) is similar to the energy difference between the barycenters of the emission bands (694 cm^{-1}) within the experimental resolution used in obtaining the spectra (1 nm). This ΔE value for Er^{3+} in different host materials ranges from 700 to 800 cm^{-1}.[14,53]

The thermometric performance in the calibration temperature range was evaluated by analyzing several metric parameters. Table 1 presents the calibration parameters of the dual-mode thermometer under UV and NIR excitation. The calibration linearity was evaluated using the regression coefficient (R^2), which was larger than 0.99. Temperature uncertainty (∂T), the smallest temperature change that can be detected in a given measurement, was determined from temperature readouts performed at different reference temperatures (displayed by the Peltier-based temperature controller). Temperature values were calculated from the calibration curves. The standard deviation of the resultant temperature is the experimental ∂T of the luminescent thermometer. Repeatability

Table 1. Calibration Parameters of the Dual-Mode Thermometer under UV and NIR Excitations

parameter	λ_{exc} 352 nm	λ_{exc} 980 nm
slope	-2.15×10^5 ($\pm 1.65 \times 10^3$)	2.16 (± 0.06)
intercept	7.23×10^7 ($\pm 5.04 \times 10^5$)	-1023.83 (± 19.80)
regression coefficient (R^2)	0.99965	0.99776
uncertainty (∂T)	0.06 K	0.47 K
repeatability (RSD)	0.32%	0.33%
relative sensitivity (S_r) at 303 K	2.67%·K^{-1}	1.48%·K^{-1}

refers to the variability between measurements. High repeatability was observed for both probes, as the relative standard deviations (RSD) among measurements values were found to be lower than 0.3%.

In addition, the accuracy was estimated to evaluate the performance of the proposed nanothermometer. For each temperature, the average value for five replicate measurements was calculated and then compared with the reference temperature. The linear function between the real and the calculated temperature revealed excellent linearity (R^2 > 0.99), indicating the closeness between the measured value and the true value.

The relative thermal sensitivity (S_r) is the parameter that describes the performance of a luminescent thermometer and allows the comparison of different types of thermometers.[9] S_r gives the variation of the experimental parameter (Q) per degree of temperature, which corresponds to (i) the FIR, for the ratiometric thermometer and (ii) the integrated intensity for the nonratiometric thermometer. S_r can be expressed as eq 2
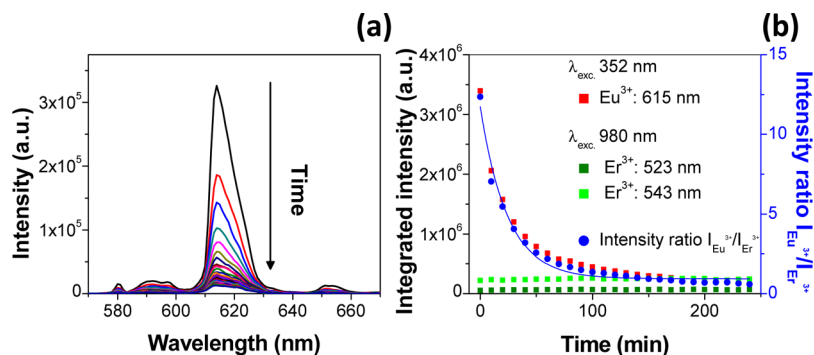
Figure 4. (a) Emission spectra (λ_{exc} 352 nm) of UCNPs@SiO$_2$−Eu(tta)$_3$ after different periods of exposure to UV light. (b) Fluorescence intensity (integrated area) under UV (352 nm) and NIR (980 nm) excitation and fluorescence intensity ratio between Eu^{3+} and Er^{3+} emissions vs time (the solid line represents the exponential fit curve).

$$S_r = \frac{(\partial Q/\partial T)}{Q} \tag{2}$$

S_r values were estimated from the calibration data (Figure 3c,d). The relative sensitivity at 303 K was 2.67%·K^{-1} for the Eu^{3+} emission and 1.48%·K^{-1} for the Er^{3+} emission. Therefore, both techniques present high relative thermal sensitivities (>1%·K^{-1}).[54]

To further investigate the behavior of NaGdF$_4$:Yb^{3+}:Er^{3+}@SiO$_2$−Eu(tta)$_3$ nanoparticles under UV-light exposure (λ = 352 nm, with a power density of 1.35 mW/cm^2), emission spectra were measured at room temperature (Figure 4a) and 980 nm after different periods of exposure to UV light. The Eu^{3+} emission intensity at 615 nm (integrated area) decay with exposure time is presented in Figure 4b. Er^{3+} emission intensities at approximately 523 and 543 nm are also represented in Figure 4b. They remained constant, showing that the upconversion thermometer was not affected by UV-light irradiation. The ratio between the Eu^{3+} and Er^{3+} emission intensities presents an exponential decay (Figure 4b) with exposure time (R^2 = 0.98294). The ratio of the Eu^{3+} downshifting emission intensity to the upconverted emission intensity is therefore sensitive to the UV exposure dose.

4. CONCLUSIONS

NaGdF$_4$:Yb^{3+}:Er^{3+} upconverting nanocrystals were obtained in the hexagonal phase by using the thermal decomposition method. The hydrophobic oleate-capped nanocrystals were coated with a thin silica shell through a reverse microemulsion route to achieve water dispersibility. The silica shell was also useful as a matrix for the incorporation of the europium(III)−tta complex. Thermal dependences of the Eu^{3+} and Er^{3+} luminescence were investigated under ultraviolet and infrared excitations. The optical thermometers so obtained presented suitable properties for use as a temperature sensor close to the physiological range (293−323 K) with excellent linearity (R^2 > 0.99). The ability to detect temperature was estimated by the calculation of thermal sensitivity. Both systems presented high thermal sensitivities (>1.5%·K^{-1}). In addition, the europium-(III) complex incorporated in the silica shell of UCNPs was found to be sensitive to ultraviolet light, which leads to its application as a UV-light sensor with no influence on the thermometer operation based on the upconversion emission. The results presented in this work stimulate the study of multifunctional materials for sensing applications based on lanthanide luminescence. The material shows potential for

application in light-activated therapies, such as photodynamic therapy (PDT) and photothermal therapy (PTT). These therapies typically require UV or blue light for excitation. The control of light dose released to the tissue is of great importance in these therapeutic procedures to avoid photo-damage to the surroundings. Moreover, as temperature is a fundamental parameter in events that occur in cells, the thermometer function is useful to guide such therapeutic processes (PDT and PTT) synergistically with the UV dosimeter.

■ AUTHOR INFORMATION

Corresponding Author
*E-mail: sjlribeiro@gmail.com.

ORCID ⓘ
Denis Boudreau: 0000-0001-5152-2464
Sidney J. L. Ribeiro: 0000-0002-8162-6747

Notes
The authors declare no competing financial interest.

■ REFERENCES

(1) Yiu, H. H. P.; Niu, H.-j.; Biermans, E.; van Tendeloo, G.; Rosseinsky, M. J. Designed multifunctional nanocomposites for biomedical applications. *Adv. Funct. Mater.* **2010**, *20*, 1599−1609.

(2) Deng, Y.; Cai, Y.; Sun, Z.; Liu, J.; Liu, C.; Wei, J.; Li, W.; Liu, C.; Wang, Y.; Zhao, D. Multifunctional mesoporous composite micro-spheres with well-designed nanostructure: A highly integrated catalyst system. *J. Am. Chem. Soc.* **2010**, *132*, 8466−8473.

(3) Guo, S.; Dong, S. Metal nanomaterial-based self-assembly: Development, electrochemical sensing and SERS applications. *J. Mater. Chem.* **2011**, *21*, 16704−16716.

(4) Rolison, D. R.; Long, J. W.; Lytle, J. C.; Fischer, A. E.; Rhodes, C. P.; Mcevoy, T. M.; Bourg, M. E.; Lubers, A. M. Multifunctional 3D nanoarchitectures for energy storage and conversion. *Chem. Soc. Rev.* **2009**, *38*, 226−252.

(5) Ribeiro, S. J. L.; dos Santos, M. V.; Silva, R. R.; Pecoraro, E.; Gonçalves, R. R.; Caiut, J. M. A. Optical properties of luminescent materials. In *The Sol−Gel Handbook, Synthesis, Characterization and*

Applications; Levy, D., Zayat, M., Eds.; Wiley-VCH Verlag GmbH & Co. KGaA: Boschstr, Weinheim, 2015; Vol. 2, pp 929−962.

(6) Bünzli, J.-C. G.; Piguet, C. Taking advantage of luminescent lanthanide ions. *Chem. Soc. Rev.* **2005**, *34*, 1048−1077.

(7) Bünzli, J.-C. G.; Eliseeva, S. V. Intriguing aspects of lanthanide luminescence. *Chem. Sci.* **2013**, *4*, 1939−1949.

(8) Carlos, L. D.; Ferreira, R. A. S.; de Zea Bermudez, V.; Ribeiro, S. J. L. Lanthanide-containing light-emitting organic−inorganic hybrids: A bet on the future. *Adv. Mater.* **2009**, *21*, 509−534.

(9) *Thermometry at the nanoscale: Technique and selected applications*; Carlos, L. D., Palacio, F., Eds.; Royal Society of Chemistry: Oxfordshire, 2016.

(10) Brites, C. D. S.; Lima, P. P.; Silva, N. J. O.; Millán, A.; Amaral, V. S.; Palacio, F.; Carlos, L. D. Thermometry at the nanoscale. *Nanoscale* **2012**, *4*, 4799−4829.

(11) Jaque, D.; Vetrone, F. Luminescence nanothermometry. *Nanoscale* **2012**, *4*, 4301−4326.

(12) Zohar, O.; Ikeda, M.; Shinagawa, H.; Inoue, H.; Nakamura, H.; Elbaum, D.; Alkon, D. L.; Yoshioka, T. Thermal imaging of receptor-activated heat production in single cells. *Biophys. J.* **1998**, *74*, 82−89.

(13) Rohani, S.; Quintanilla, M.; Tuccio, S.; De Angelis, F.; Cantelar, E.; Govorov, A. O.; Razzari, L.; Vetrone, F. Enhanced luminescence, collective heating, and nanothermometry in an ensemble system composed of lanthanide-doped upconverting nanoparticles and gold nanorods. *Adv. Opt. Mater.* **2015**, *3*, 1606−1613.

(14) Debasu, M. L.; Brites, C. D. S.; Balabhadra, S.; Oliveira, H.; Rocha, J.; Carlos, L. D. Nanoplatforms for plasmon-induced heating and thermometry. *ChemNanoMat* **2016**, *2*, 520−527.

(15) Mecklenburg, M.; Hubbard, W. A.; White, E. R.; Dhall, R.; Cronin, S. B.; Aloni, S.; Regan, B. C. Nanoscale temperature mapping in operating microelectronic devices. *Science* **2015**, *347*, 629−632.

(16) Yarimaga, O.; Lee, S.; Ham, D.-Y.; Choi, J.-M.; Kwon, S. G.; Im, M.; Kim, S.; Kim, J.-M.; Choi, Y.-K. Thermofluorescent conjugated polymer sensors for nano- and microscale temperature monitoring. *Macromol. Chem. Phys.* **2011**, *212*, 1211−1220.

(17) Brites, C. D. S.; Xie, X.; Debasu, M. L.; Qin, X.; Chen, R.; Huang, W.; Rocha, J.; Liu, X.; Carlos, L. D. Instantaneous ballistic velocity of suspended Brownian nanocrystals measured by upconversion nanothermometry. *Nat. Nanotechnol.* **2016**, *11*, 851−856.

(18) Zhang, F. *Photon Upconversion Nanomaterials*; Springer-Verlag: Berlin, 2015; pp 343−374.

(19) Menezes, L. D. S.; Araújo, C. B. D. Optically detected thermal effects in rare-earth doped materials for host characterization, thermometric devices, nanothermometry and biothermometry. *J. Braz. Chem. Soc.* **2015**, *26*, 2405−2417.

(20) *Phosphors, up conversion nano particles, quantum dots and their applications*; Liu, R.-S., Ed.; Springer: Singapore, 2016; Vol. 2.

(21) Rocha, U.; Jacinto, C.; Kumar, K. U.; López, F. J.; Bravo, D.; Solé, J. G.; Jaque, D. Real-time deep-tissue thermal sensing with sub-degree resolution by thermally improved Nd^{3+}:LaF$_3$ multifunctional nanoparticles. *J. Lumin.* **2016**, *175*, 149−157.

(22) Nunes, L. A. O.; Souza, A. S.; Carlos, L. D.; Malta, O. L. Neodymium doped fluoroindogallate glasses as highly-sensitive luminescent non-contact thermometers. *Opt. Mater.* **2017**, *63*, 42−45.

(23) Peng, H.; Stich, M. I. J.; Yu, J.; Sun, L.-N.; Fischer, L. H.; Wolfbeis, O. S. Luminescent europium(III) nanoparticles for sensing and imaging of temperature in the physiological range. *Adv. Mater.* **2010**, *22*, 716−719.

(24) Suzuki, M.; Tseeb, V.; Oyama, K.; Ishiwata, S. Microscopic detection of thermogenesis in a single HeLa cell. *Biophys. J.* **2007**, *92*, L46−L48.

(25) Oyama, K.; Takabayashi, M.; Takei, Y.; Arai, S.; Takeoka, S.; Ishiwata, S.; Suzuki, M. Walking nanothermometers: Spatiotemporal temperature measurement of transported acidic organelles in single living cells. *Lab Chip* **2012**, *12*, 1591−1593.

(26) Takei, Y.; Arai, S.; Murata, A.; Takabayashi, M.; Oyama, K.; Ishiwata, S.; Takeoka, S.; Suzuki, M. A nanoparticle-based ratiometric and self-calibrated fluorescent thermometer for single living cells. *ACS Nano* **2014**, *8*, 198−206.

(27) Shahi, P. K.; Singh, A. K.; Singh, S. K.; Rai, S. B.; Ullrich, B. Revelation of the technological versatility of the Eu(TTA)$_3$Phen complex by demonstrating energy harvesting, ultraviolet light detection, temperature sensing, and laser applications. *ACS Appl. Mater. Interfaces* **2015**, *7*, 18231−18239.

(28) Shahi, P. K.; Singh, A. K.; Rai, S. B.; Ullrich, B. Lanthanide complexes for temperature sensing, UV light detection, and laser applications. *Sens. Actuators, A* **2015**, *222*, 255−261.

(29) Nockemann, P.; Beurer, E.; Driesen, K.; Van Deun, R.; Van Hecke, K.; Van Meervelt, L.; Binnemans, K. Photostability of a highly luminescent europium β-diketonate complex in imidazolium ionic liquids. *Chem. Commun.* **2005**, 4354−4356.

(30) Pagnot, T.; Audebert, P.; Tribillon, G. Photostability study of europium dibenzoylmethide embedded in polystyrene thin films with high concentration. *Chem. Phys. Lett.* **2000**, *322*, 572−578.

(31) Kai, J.; Felinto, M. C. F. C.; Nunes, L. A. O.; Malta, O. L.; Brito, H. F. Intermolecular energy transfer and photostability of luminescence-tuneable multicolour PMMA films doped with lanthanide−β-diketonate complexes. *J. Mater. Chem.* **2011**, *21*, 3796−3802.

(32) Quirino, W.; Reyes, R.; Legnani, C.; Nóbrega, P. C.; Santa-Cruz, P. A.; Cremona, M. Eu-β-diketonate complex OLED as UV portable dosimeter. *Synth. Met.* **2011**, *161*, 964−968.

(33) Sousa, F. L. N.; Mojica-Sánchez, L. C.; Gavazza, S.; Florencio, L.; Vaz, E. C. R.; Santa-Cruz, P. A. Printable UV personal dosimeter: Sensitivity as a function of DoD parameters and number of layers of a functional photonic ink. *Mater. Res. Express* **2016**, *3*, 045701.

(34) Wei, C.; Wei, H.; Yan, W.; Zhao, Z.; Cai, Z.; Sun, B.; Meng, Z.; Liu, Z.; Bian, Z.; Huang, C. Water-soluble and highly luminescent Europium(III) complexes with favorable photostability and sensitive pH response behavior. *Inorg. Chem.* **2016**, *55*, 10645−10653.

(35) Liu, Y.; Qian, G.; Wang, Z.; Wang, M. Temperature-dependent luminescent properties of Eu−Tb complexes synthesized in situ in gel glass. *Appl. Phys. Lett.* **2005**, *86*, 071907.

(36) Marciniak, Ł.; Bednarkiewicz, A.; Stefanski, M.; Tomala, R.; Hreniak, D.; Strek, W. Near infrared absorbing near infrared emitting highly-sensitive luminescent nanothermometer based on Nd^{3+} to Yb^{3+} energy transfer. *Phys. Chem. Chem. Phys.* **2015**, *17*, 24315−24321.

(37) Brites, C. D. S.; Lima, P. P.; Silva, N. J. O.; Millán, A.; Amaral, V. S.; Palacio, F.; Carlos, L. D. A. A Luminescent molecular thermometer for long-term absolute temperature measurements at the nanoscale. *Adv. Mater.* **2010**, *22*, 4499−4504.

(38) Gorris, H. H.; Ali, R.; Saleh, S. M.; Wolfbeis, O. S. Tuning the dual emission of photon-upconverting nanoparticles for ratiometric multiplexed encoding. *Adv. Mater.* **2011**, *23*, 1652−1655.

(39) Cerón, E. N.; Ortgies, D. H.; del Rosal, B.; Ren, F.; Benayas, A.; Vetrone, F.; Ma, D.; Sanz-Rodríguez, F.; Solé, J. G.; Jaque, D.; Rodríguez, E. M. Hybrid nanostructures for high-sensitivity luminescence nanothermometry in the second biological window. *Adv. Mater.* **2015**, *27*, 4781−4787.

(40) Chen, D.; Liu, S.; Wan, Z.; Ji, Z. EuF$_3$/Ga$_2$O$_3$ Dual-Phase Nanostructural Glass Ceramics with Eu^{2+}/Cr^{3+} Dual-Activator Luminescence for Self-Calibrated Optical Thermometry. *J. Phys. Chem. C* **2016**, *120*, 21858−21865.

(41) Chen, D.; Wan, Z.; Zhou, Y.; Zhou, X.; Yu, Y.; Zhong, J.; Ding, M.; Ji, Z. Dual-phase glass ceramic: Structure, dual-modal luminescence, and temperature sensing behaviors. *ACS Appl. Mater. Interfaces* **2015**, *7*, 19484−19493.

(42) Chen, D.; Wan, Z.; Liu, S. highly sensitive dual-phase nanoglass-ceramics self-calibrated optical thermometer. *Anal. Chem.* **2016**, *88*, 4099−4106.

(43) Chen, D.; Wan, Z.; Zhou, Y. Dual-phase nano-glass-ceramics for optical thermometry. *Sens. Actuators, B* **2016**, *226*, 14−23.

(44) Xu, M.; Chen, D.; Huang, P.; Wan, Z.; Zhou, Y.; Ji, Z. A dual-functional upconversion core@shell nanostructure for white-light-emission and temperature sensing. *J. Mater. Chem. C* **2016**, *4*, 6516−6524.

(45) Marciniak, L.; Bednarkiewicz, A. Nanocrystalline NIR-to-NIR luminescent thermometer based on Cr^{3+},Yb^{3+} emission. *Sens. Actuators, B* **2017**, *243*, 388−393.

(46) Marciniak, L.; Bednarkiewicz, A.; Kowalska, D.; Strek, W. A new generation of highly sensitive luminescent thermometers operating in the optical window of biological tissues. *J. Mater. Chem. C* **2016**, *4*, 5559−5563.

(47) Zhou, J.; Liu, Z.; Li, F. Upconversion nanophosphors for small-animal imaging. *Chem. Soc. Rev.* **2012**, *41*, 1323−1349.

(48) Hemmer, E.; Quintanilla, M.; Légaré, F.; Vetrone, F. Temperature-induced energy transfer in dye-conjugated upconverting nanoparticles: A new candidate for nanothermometry. *Chem. Mater.* **2015**, *27*, 235−244.

(49) Li, Z.; Zhang, Y.; Jiang, S. Multicolor core/shell-structured upconversion fluorescent nanoparticles. *Adv. Mater.* **2008**, *20*, 4765−4769.

(50) Li, C.; Hou, Z.; Dai, Y.; Yang, D.; Cheng, Z.; Ma, P.; Lin, J. A facile fabrication of upconversion luminescent and mesoporous core−shell structured β-NaYF$_4$:Yb^{3+}, Er^{3+}@mSiO$_2$ nanocomposite spheres for anti-cancer drug delivery and cell imaging. *Biomater. Sci.* **2013**, *1*, 213−223.

(51) Kostiv, U.; Janoušková, O.; Šlouf, M.; Kotov, N.; Engstová, H.; Smolková, K.; Ježek, P.; Horák, D. Silica-modified monodisperse hexagonal lanthanide nanocrystals: Synthesis and biological properties. *Nanoscale* **2015**, *7*, 18096−18104.

(52) Molina, C.; Dahmouche, K.; Messaddeq, Y.; Ribeiro, S. J. L.; Silva, M. A. P.; de Zea Bermudez, V.; Carlos, L. D. Enhanced emission from Eu(III) β-diketone complex combined with ether-type oxygen atoms of di-ureasil organic−inorganic hybrids. *J. Lumin.* **2003**, *104*, 93−101.

(53) Debasu, M. L.; Ananias, D.; Pastoriza-Santos, I.; Liz-Marzán, L. M.; Rocha, J.; Carlos, L. D. All-in-one optical heater-thermometer nanoplatform operative from 300 to 2000 K Based on Er^{3+} Emission and Blackbody Radiation. *Adv. Mater.* **2013**, *25*, 4868−4874.

(54) Brites, C. D. S.; Millán, A.; Carlos, L. D. Lanthanides in luminescent thermometry. In *Handbook on the Physics and Chemistry of Rare Earths*; Bünzli, J. C. G., Pecharsky, V. K., Eds.; Elsevier B.V.: Amsterdam, 2016; Vol. *49*, pp 339−427.